Exploring the Surface Chemistry of Cesium Lead Halide Perovskite Nanocrystals

Roberto Grisorio,[a,b] *Milvia Elena Di Clemente,*[c] *Elisabetta Fanizza,*[c,d] *Ignazio Allegretta,*[e] *Davide Altamura,*[f] *Marinella Striccoli,*[c,d] *Roberto Terzano,*[e] *Cinzia Giannini,*[f] *Mihai Irimia-Vladu,*[g] *Gian Paolo Suranna*[a,b]

[a]*Dipartimento di Ingegneria Civile, Ambientale, del Territorio, Edile e di Chimica (DICATECh), Politecnico di Bari, Via Orabona 4, 70125 Bari, Italy.* E-mail: roberto.grisorio@poliba.it

[b]*CNR NANOTEC − Istituto di Nanotecnologia, Via Monteroni, 73100 Lecce, Italy.*

[c]*Dipartimento di Chimica, Università degli Studi di Bari " A. Moro", Via Orabona 4 , 70126 Bari, Italy.*

[d]*CNR-Istituto per i Processi Chimico Fisici, UOS Bari, Via Orabona 4 , 70126 Bari, Italy.*

[e]*Dipartimento di Scienze del Suolo, della Pianta e degli Alimenti, Università degli Studi di Bari "Aldo Moro", Via G. Amendola 165/A, 70126 Bari, Italy.*

[f]*Institute of Crystallography, National Research Council, via Amendola 122/O, Bari 70126, Italy.*

[g]*Joanneum Research MATERIALS - Institute for Surface Technologies and Photonics, Franz-Pichler Straße 30, Weiz A-8160, Austria.*

ABSTRACT

Colloidal nanocrystals (NCs) of cesium lead halide perovskites ($CsPbX_3$, X = Cl, Br or I) are emerging as an exciting class of optoelectronic materials, but the retention of their colloidal and structural integrity during isolation, purification and handling still represents a critical issue. The impelling questions concerning their intrinsic chemical instability are connected to the dynamic nature of the bonding between the inorganic surface and the long-chain capping ligands. However, the key aspects of $CsPbX_3$ surface chemistry directly impacting on their stability remain elusive. In this contribution, we provide an in-depth investigation of the surface properties of differently composed $CsPbX_3$ NCs, prepared by traditional hot-injection methods. The study, mainly relying on solution NMR spectroscopy, is backed up by elemental analysis as well as morphological, structural and optical investigations. We ascertained how the nature of ligand adsorption/desorption processes at the NC surface is dependent on its elemental composition, thus understanding the origin of the instability afflicting $CsPbI_3$ NCs. We also evaluated the role of NC purification as well as of the degradation pathways involving the organic shell on the surface chemistry of $CsPbX_3$ NCs. This study paves the way towards new post-functionalization strategies for this promising class of nanomaterials.

INTRODUCTION

While semiconducting metal halide perovskites are strengthening their huge potential in photovoltaics[1] and light-emitting devices,[2] perovskite nanocrystals (NCs) have recently emerged as outstanding alternatives for optoelectronic applications.[3] In particular, all-inorganic cesium lead halide perovskite NCs[4] (with formula $CsPbX_3$ in which X can be Cl, Br, or I) displayed excellent photophysical properties associated to quantum confinement[5] comprising high photoluminescence (PL) quantum yields and narrow emission peak widths.[6] By adjusting their dimensions as well as halide composition,[7] the emission of these materials can potentially span from the ultraviolet to the near-infrared region.[8]

Unfortunately, in spite of their promises, the chemical and colloidal instability of $CsPbX_3$ NCs when exposed to polar solvents or moisture *de facto* precludes their vast utilization.[9] With respect to the widely known chalcogenide quantum dots,[10] the crystal structure of $CsPbX_3$ NCs exhibits a more predominant ionic character, which consequently dominates the interactions with the organic shell, making labile the ligand-NC bonds responsible for the passivation of the inorganic framework.[11] This peculiarity of $CsPbX_3$ affects their colloidal stability and, in some cases, their structural integrity, mainly when the perovskite NCs get in touch with polar solvents tentatively added to isolate and/or purify the nanoparticles.[12] The poor structural stability is particularly evident in the case of $CsPbI_3$ NCs, in which the degradation process leads to the phase transformation into a non-perovskite material.[13] Several approaches have been conceived for the stabilization of $CsPbI_3$ cubic phase, such as the substitution of cesium cations with formamidinium ones[14] and the use of alkyl phosphonic acids,[15] phosphines[16] or benzoyl iodide[17] during the synthesis without post-synthesis treatments. Based on these findings, it can be suspected that the phase instability of $CsPbI_3$ NCs (and generally of $CsPbX_3$ nanoparticles) is related to surface chemistry of the nanoparticle. However, understanding the structure of nanoscale interfaces requires an elaborate mix of concepts and techniques borrowed from surface science and coordination chemistry.

The NC surface is protected by the ligands, *i.e.* molecules that bind to the surface, which, as critical components of NC synthesis, not only influence the nucleation process preventing inter-particle aggregation, but also determine the physical and chemical behaviour of the resulting nanoparticles. Conventionally, oleic acid (OLA) and oleylamine (OAM) ligands are used in the preparation of $CsPbX_3$ NCs. It has been suggested that oleylammonium halides are the main surface passivating agents of $CsPbX_3$ NCs,[18,19]while the role in passivation by OLA is still under debate. However, recent investigations are elucidating the crucial function exerted by OLA[20] and OAM[21] on the transformations of perovskite NCs with degradation of their structural and optical properties. Furthermore, common capping ligands act as electrically insulating layers on the NC surface, which significantly hinder charge carrier injection and transport at the interface in optoelectronic devices.[22] All these observations point to a comprehensive investigation of $CsPbX_3$ surface chemistry to plan effective functionalization and to evaluate its effects on NC surface and stability.

Nuclear magnetic resonance (NMR) spectroscopy constitutes an ideal technique to study the details of the NC organic-inorganic interface unraveling the ligand shell composition and suggesting its binding motifs.[23] The combination of ^{1}H-NMR, nuclear Overhauser effect spectroscopy (NOESY) and diffusion ordered spectroscopy (DOSY) allows to clearly discriminate the dynamics of the adsorption/desorption processes involving the passivating agents.[24] Sharp resonances with negative nuclear Overhauser effect (nOe) cross peaks and fast diffusion coefficients are actually produced by weakly bound ligands resulting from a fast adsorption/desorption process at NC surface. Conversely, broadened resonances with negative nOe peaks and slow diffusion coefficients are due to tightly bound ligands not (or slowly) exchanging with free species.[25]

Here, we focus on inorganic $CsPbX_3$ NCs synthesized by the traditional hot-injection approaches to deeply investigate the impact of a different halide composition on their surface chemistry *via* solution ^{1}H-NMR techniques. Our studies indicate that, although with different contributions, both aliphatic carboxylic acids and amines used for the nanoparticle synthesis participate to the surface

passivation of as-prepared perovskite NCs. However, the equilibria involved in the passivation process were found to be dependent on the NC composition and solvent, thus explaining the differences in stability observed for $CsPbX_3$ nanoparticles. We believe that the details on the degradation mechanism involving the common NC organic shell could inspire efforts for surface modifications required for the optoelectronic applications of these exciting nanomaterials.

RESULTS AND DISCUSSION

Synthesis and characterization of $CsPbX_3$ NCs. As specified in the Experimental Section, perovskite $CsPbX_3$ NCs (X = Cl, Br, I, and mixed Br/Cl, I/Br) were prepared by following the synthetic procedure reported by Protesescu *et al.*[8] In brief, the relevant lead-halides (0.38 mmol) were dissolved in 7.5 mL of octadecene (ODE) containing 1.0 mL of each ligand (OAM and OA). After the PbX_2 was dissolved at the chosen reaction temperature (160 °C), a warm Cs-oleate (0.09 mmol) solution was injected. The obtained mixture was rapidly cooled (< 10 sec) with an ice bath and centrifugated for the product isolation. The mixed-halide perovskite NCs were synthesized by mixing an equimolar ratio of the suitable lead halides under the same reaction conditions and their formal composition, based on the molar feed ratio is reported in Table 1. In all cases, it can be assumed that the centrifugation allows to recover most of the perovskite NCs as precipitate, as testified by the observation that the supernatant liquid after centrifugation is barely colored and non-fluorescent. At this stage, the isolated perovskite nanoparticles probably include an indefinite amount of remnant synthetic precursors and solvent. While the purification by multiple precipitation/redispersion steps using polar solvents (such as ethanol, methanol, acetone, or ethyl acetate) is common practice in the course of NC preparation, the isolation of the $CsPbX_3$ NCs in polar media often compromises their colloidal stability. We decided to gain insights into the effects of purification on the NC surface chemistry by using solution NMR spectroscopy (*vide infra*). The products collected from the first centrifugation were dispersed in hexane (1.2 mL), precipitated with

acetone (1.2 mL) and recovered by a further centrifugation. The addition of 50 μL of both ligands prior to precipitation with acetone was crucial to maintain the colloidal stability of our $CsPbX_3$ NCs, except for $CsPbI_3$, for which the interaction with the polar solvent immediately caused its phase deterioration leading to an insoluble material.

Molar feed ratio	**Sample**	**Elemental composition**	**Dimension (nm)**	**UV-Vis onset (nm)**	**λ_{em} (nm)**	**FWHM (nm)**	**PLQY (%)**
$CsPbCl_3$	as-prep	$Cs_{1.1}PbCl_{3.1}$	9.3±1.8	386	401	14	0.3
$CsPbCl_{1.5}Br_{1.5}$	as-prep	$Cs_{1.1}PbCl_{1.6}Br_{1.4}$	7.1±0.9	437	452	20	5
$CsPbCl_{1.5}Br_{1.5}$	pur	$Cs_{1.3}PbCl_{1.5}Br_{1.4}$	7.6±1.3	441	455	17	2
$CsPbBr_3$	as-prep	$Cs_{1.2}PbBr_{2.8}$	9.0±0.8	502	513	21	74
$CsPbBr_3$	pur	$Cs_{1.3}Pb\ Br_{2.8}$	10.9±1.1	501	516	16	74
$CsPbBr_{1.5}I_{1.5}$	as-prep	$Cs_{1.4}PbBr_2I_{1.4}$	9.7±1.5	547	576	35	39
$CsPbBr_{1.5}I_{1.5}$	pur	$Cs_{1.3}PbBr_{2.6}I_{0.6}$	11.3±1.4	523	533	27	32
$CsPbI_3$	as-prep	$Cs_{1.3}PbI_{3.7}$	8.0±1.3	651	669	39	53

Table 1. *Summary of the elemental composition, morphological (TEM) and optical properties (cyclohexane) of $CsPbX_3$ NCs.*

The success of this purification protocol motivated us to attempt a further washing step using the same procedure on $CsPbBr_3$ NCs. Unfortunately, the colloidal stability of the resulting material was, in this case, severely compromised. Probably, desorption of the protective ligand shell upon drastic purification leads to the loss of NC structural integrity, *i.e.* aggregation of NCs into bulk polycrystalline materials. Hence, only a single purification step is applicable, which preserves colloidal stability of the resulting NCs.

The size and morphology of as-prepared $CsPbX_3$ NCs were investigated by transmission electron microscopy (TEM), which clearly evidences predominant fraction of well defined square shaped

nanostructures, ascribable to nanocubes for our perovskite nanomaterials (Figure 1A-F and Figure S1). Their average sizes are reported in Table 1. It can be observed that the purification step preserves the NCs morphology, while slightly increasing their average sizes, which suggests a sort of reorganization of the nanoparticles, as also confirmed by the structural analysis. The optical response of the obtained $CsPbX_3$ NCs was quantified by absorption measurements; their PL emission wavelength spanned the entire visible range (from 401 to 684 nm) by adjusting the halide composition (Figure 1G).[26] Since previous studies assessed that the precipitation with an antisolvent has a large impact on optical properties of the resulting NCs,9 we compared the emission properties of the as-prepared products with those of the relevant purified samples in the case of $CsPb(Br/Cl)_3$, $CsPbBr_3$ and $CsPb(I/Br)_3$ nanoparticles. As a general consideration, both as-prepared and purified $CsPbX_3$ solutions exhibits relatively narrow (FWHM of 14÷39 nm) and single-peak PL emission with small Stokes shifts, as evidenced in Table 1. While these observations point to a single halide composition for mixed-halide perovskite NCs, it can be noted that the purification procedure heavily affects only the PL behaviour of the mixed-halide $CsPb(I/Br)_3$ nanoparticles. In the case of $CsPb(I/Br)_3$ NCs, the purification method preserves their shape integrity, as confirmed by TEM investigations, but both absorption and emission maxima are remarkably blue-shifted by the treatment with the polar solvent (Figure 1H and Table 1). In the case of the other perovskite NCs submitted to a single purification step – *i.e.* $CsPb(Br/Cl)_3$ and $CsPbBr_3$ – we observed that the optical properties (absorption, emission and quantum yield) remained almost unaltered upon purification. The slight red-shift of the emission in purified samples is due to the fact that the smallest NCs are apparently removed in the washing procedure, as supported by the observation that the centrifugation supernatant of $CsPbBr_3$ NCs (opportunely diluted in cyclohexane) shows an intense and blue-shifted emission (λ_{em} = 498 nm) with respect to that of as-prepared samples (Figure S2). As a consequence, the full-width at half maximum (FWHM) of the emission bands results to be smaller in the case of purified samples. Moreover, all samples exhibit high PL quantum yields, differently from what observed for chlorine-containing NCs (Table 1).

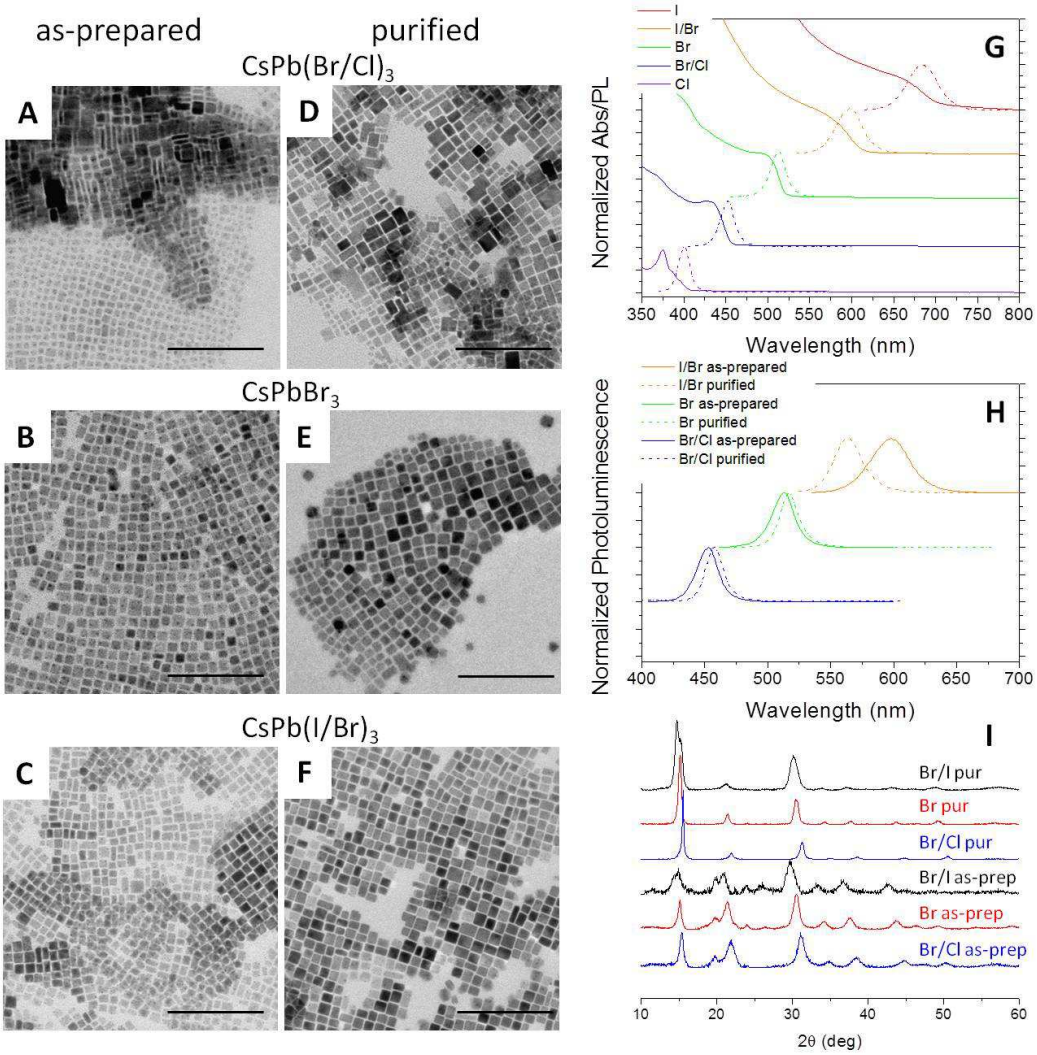

Figure 1. *TEM micrographs of as-prepared $CsPb(Br/Cl)_3$ (A), $CsPbBr_3$ (B), $CsPb(I/Br)_3$ (C) NCs and the relevant purified samples (D-F). Scale bar = 100 nm. (G) UV/Vis absorption and PL spectra of as-prepared $CsPbCl_3$, $CsPb(Br/Cl)_3$, $CsPbBr_3$, $CsPb(I/Br)_3$ and $CsPbI_3$ NCs obtained by hot injection at 160 °C. (H) Comparison between PL spectra of as-prepared and purified NCs shown in TEM images and (I) XRD patterns of the same samples. UV-Vis and PL have been recorded in cyclohexane.*

From the structural point of view, the XRD patterns (detector scan) reported in Fig. 1I clearly show the effect of purification, as all purified and as-prepared samples feature similar patterns,

respectively. In particular, Le Bail-based whole pattern analysis with EXPO[27] revealed a $CsPbX_3$ single phase with a distorted cubic symmetry in the purified samples, which is also present in the as-prepared ones along with an additional crystalline phase giving rise to extra peaks. The main peaks at about 2θ = 15° and 31° would be the first and second diffraction orders of the *l00* reflections in the cubic system according to the ICSD #201285 powder diffraction file. However, because of peak broadening due to the small NC size, it is hard to unambiguously discriminate among other possible crystal phases often reported in literature, such as monoclinic or orthorhombic, with similar cell parameters, therefore we discuss our results taking into account the different reported crystallographic datasheets for the sake of completeness. Moreover, relative intensities are likely affected by NC preferred orientation, which can be expected to be face on in the case of cube shaped nanoparticles. Compared to the more surface sensitive detector scans (fixed 0.5° incidence angle) reported in Fig. 1I, the coupled sample-detector (θ/2θ) scans reported in Figure S3 provide thus more reliable relative intensities for the *l*00 peaks (as they are collected from the very same lattice planes), besides a better angular resolution. Purified $CsPbBr_3$ and $CsPb(Br/Cl)_3$ samples show a clear single phase pattern: the former being compatible with the monoclinic or orthorhombic phases (JCPDS #18-0364 and ICDD #01-072-7929, respectively), both featuring a doublet at 2θ = 30.4° / 30.7°; the latter, featuring a single peak at 2θ = 31.4°, being compatible with the cubic phase. The ratio between the integrated areas under the two main peaks is (1.2) closer to that of the monoclinic phase (1.1 in JCPDS #18-0364) in the as-prepared $CsPbBr_3$ sample (not shown), between the monoclinic and the orthorhombic phase value (1.8 in ICDD #01-072-7929) in the purified $CsPbBr_3$ sample, closer to the cubic phase (expected ratio 1.3 - JCPDS #18-0464 to 2.3 - ICDD # 01-072-7930 and JCPDS # 75-0412) in the purified $CsPb(Br/Cl)_3$ samples (1.7). On the other hand, purified $CsPb(I/Br)_3$ samples show further diffraction contributions convoluted with the first main peak, indicating a possible non-complete phase purification.

At the same time, it should be emphasized that our purified $CsPbBr_3$ and the corresponding mixed-halide NCs exhibit an good stability when exposed at ambient conditions, also after solvent evaporation. After being stored for three weeks in ambient conditions, the as-prepared $CsPbBr_3$ NCs appeared as a yellow solid, while the purified ones maintained their colloidal integrity (Figure S4). To explain this behaviour, an insight was needed into the surface chemistry of lead halide-based perovskite NCs, which is well known to play a crucial role in determining not only their optical performance,[28] but also their stability in air.[29]

To deepen this aspect, we firstly analyzed the composition of both as-prepared and purified samples *via* energy dispersive X-ray spectroscopy (EDX) coupled with field emission gun scanning electron microscopy (FEG-SEM). The relevant results in terms of the NC elemental composition are listed in Table 1 (see also Table S1 and Figure S5). All our $CsPbX_3$ NCs show an excess cesium with respect to lead, supporting the hypothesis that these nanoparticles exhibit Cs-exposed surfaces, despite the fact that the NC syntheses were carried out using a formal excess of lead precursors (see Experimental Section). It has been ascertained that part of the surface cesium atoms can be replaced by oleylammonium ions after the NC assembly,[30] thereby explaining most of the results on $CsPbX_3$ composition exhibiting a near equimolar Cs/Pb ratio.[31] Hence, considering the relatively mild synthetic conditions preserving the thermodynamically favored oxidation state of the relevant precursors, $CsPbX_3$ nanocubes with the elemental composition obtained by our EDX data would expose oleylammonium ions, Cs^+ and halides at the surface.[32] The eventual excess of positive charge would be neutralized by oleate ions. Concerning as-prepared mixed-halide NCs, the halide composition of $CsPb(I/Br)_3$ NCs reported in Table 1 suggests that PbI_2 precursor is less reactive than the bromine-based counterpart under our reaction conditions. This behaviour was found to be remarkably different from that of $CsPb(Br/Cl)_3$ NCs, where bromide and chloride ions are incorporated within the nanoparticles in an equimolar ratio. Moreover, the elemental composition of our NCs seems to be marginally affected by the purification step, with the exception of $CsPb(I/Br)_3$

NCs, for which the Br/I molar ratio increases from 1.4 in as-prepared samples to 4.3 in purified samples, suggesting that iodide ions are removed in the course of purification.[33] In order to rationalize these observations, we explored the surface chemistry of perovskite $CsPbX_3$ NCs.

The surface chemistry of $CsPbBr_3$ NCs. Before elucidating the surface chemistry of $CsPbX_3$ NCs *via* solution NMR investigations, it is firstly convenient to report (Figure 2A) a pictorial description of all plausible equilibria involving the organic shell of the nanoparticles, based on the structural information drawn from nanomaterial characterization. Considering that our investigations have mainly been carried out on perovskite NCs which have not undergone post-synthetic purification steps, these equilibria could involve the excess ligands (OLA and OAM) or unreacted synthetic precursors (cesium oleate). In parallel, the ionic structure of perovskite NCs could promote adsorption/desorption processes of weakly bound species at the nanoparticle surface. The organic cations (oleylammonium) are kept on the surface of the inorganic framework by ionic interaction or hydrogen bonding, but their dynamic surface passivation would necessarily engage neutral species, as oleylammonium halides or OAM, to minimize the required energy for the process.[30] The passivation process involving OAM inevitably releases protons on the NC surface (as schematized in Figure 2), that could explain the catalytic activity of our nanoparticles for the amide formation from carboxylic acids and aliphatic amines (*vide infra*), as already observed for HfO_2 nanoparticles.[34] However, the interaction of the nanoparticle with protons cannot be completely supported by NMR investigations, since the possible presence of acidic protons on the NC surface is undetectable due to their fast T_2 relaxation. The superficial electron-withdrawing halide atoms could also promote the formation of hydrogen bonds with OLA, while the nitrogen lone pair of OAM could also passivate eventual undercoordinated metal atoms at the NC surface.[35] Furthermore, since elemental analyses supported the presence of cationic excess on the surface, ligand displacement involving excess OLA could be promoted by proton transfer, in analogy to

what observed for chalcogenide quantum dots.[36] As a matter of fact, the passivation process is further complicated by the acid-base equilibrium of the same ligands, on which the NC surface itself can have an influence (Figure 2B).

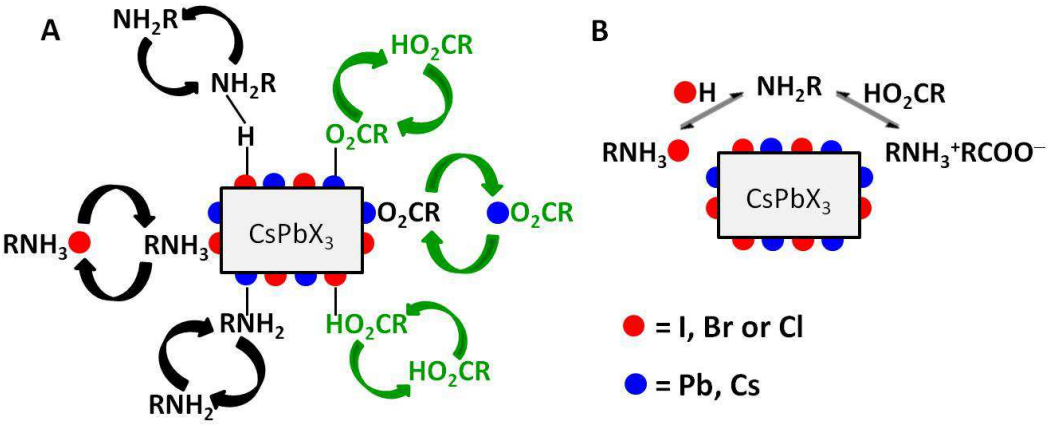

Figure 2. *(A) Schematic representation of the equilibria involving aliphatic amines and carboxylic acids as the ligands for the passivation of perovskite NC surfaces. (B) Schematic representation of the equilibria involving the ligands while engaged in the passivation process.*

On these bases, we compared the ^{1}H-NMR spectra of as-prepared $CsPbBr_3$ NCs with those of the species employed for the nanomaterial synthesis: OLA, OAM, an equivolumetric mixture of both, and Cs-oleate directly sampled from the solution used for the NC synthesis (Figure 3). The spectra were recorded in two solvents characterized by different viscosity and polarity, namely C_6D_6 and $CDCl_3$, since due to peculiar solvent-ligand interactions, the deuterated solvent strongly influences the line-broadening and chemical shift of NMR signals belonging to NC surface ligands, as recently observed by De Roo *et al.* on metal-chalcogenide and -oxide nanoparticles.[37] As a first consideration, it is evident that, independently of the solvent polarity, some NC resonances appear significantly broadened with respect to those of free OLA and OAM, reflecting their nature of organic species more or less interacting with the NC surface.[38] The broadening of the NMR ligand signals could arise from multiple effects in NCs passivated by organic species, including slow

tumbling of the large NCs, decreased spin-spin relaxation time (T_2), heterogeneity of the NCs in size, shape and surface properties. The ligand behaviour in solution can properly be scrutinized by focusing on the resonances of methylene protons adjacent to the ligand binding group, which are labeled as **1** and **β** for OLA and OAM, respectively (Figure 3). Importantly, the ^{1}H-NMR spectrum of OLA recorded in C_6D_6 is different with respect to that recorded in $CDCl_3$, being the signal of **1** remarkably downfield shifted in the polar medium. This peculiarity observed for OLA, which is also reflected in the corresponding spectrum of as-prepared $CsPbBr_3$, is likely due to the specific interactions of the carboxylic acid moiety with the solvent. By contrast, the ^{1}H-NMR spectra of OAM are very similar and not affected by solvent polarity, but the spectrum of an equimolar mixture of OLA and OAM (a mixture employed for the NC synthesis) reveals a downfield shift of the **β** resonance both in C_6D_6 and in $CDCl_3$, as a consequence of the nitrogen protonation. In the case of OLA, deprotonation causes a downfield shift of the **1** resonance in C_6D_6, while an upfield shift is observed in $CDCl_3$. This trend was also confirmed by inspecting the **1** resonance of cesium oleate solution in ODE which is employed for the NC synthesis, as a reference species for the carboxylate moiety.

Concerning as-prepared $CsPbBr_3$ NCs, the ^{1}H-NMR spectrum features prominent resonances related to OLA and OAM: the vinylene protons at δ = 5.70÷5.50 ppm (**5** and **ε**), the methylene protons next to the vinylene protons at δ = ~2.10 ppm (**4** and **δ**), an unresolved resonance at δ = ~1.50 ppm attributed to the methylene groups (**3**) and the methyl resonance (**6**) at δ = ~0.90 ppm, as sketched in Figure 3. The intensity of these protons away from the NC surface gain benefit from internal molecular motional freedom. Notwithstanding the NMR broadening is particularly severe for protons close to the NC surface, in the case of as-prepared $CsPbBr_3$ NCs we can observe the signals of the peculiar protons ascribable to the ligands (*i.e.* **1** and **β** for OLA and OAM, respectively) needed for ascertaining their behaviour in the passivation process. Since their chemical shifts are influenced by the acid-base equilibrium,[39] we can state that in the apolar solvent

OAM of as-prepared $CsPbBr_3$ NCs is partially protonated, while OLA is partially deprotonated. However, it is apparent how the signals associated to OLA (in particular **1** and **2**) are sharper and more intense with respect to the corresponding signals of OAM, hinting a higher degree of solvatation for the carboxylic acid. A similar situation crops up from the analysis of the ^{1}H-NMR spectrum of as-prepared $CsPbBr_3$ NCs in $CDCl_3$, in which the **β** signal results very broadened. In this case, however, the downfield shifted **β** resonance suggests that OAM is largely protonated, while the characteristic resonances **1** and **2** of OLA appear slightly broadened and upfield shifted with respect to the reference. These insights point to a ligand absorption on the NC surface regulated by the solvent polarity and/or viscosity, which promote different passivation mechanisms. A more detailed description of the organic shell protecting the NC surface could emerge from the analysis of the surface chemistry of $CsPbBr_3$ NCs upon purification and from observations on their stability.

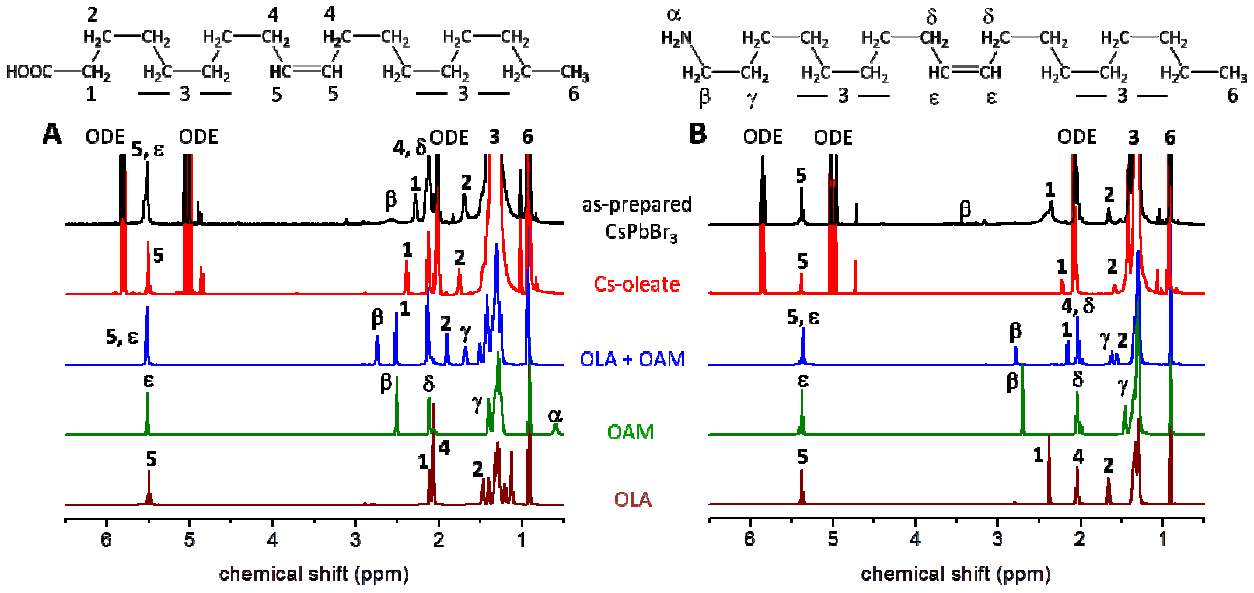

Figure 3. *^{1}H-NMR spectra of OLA (0.2M), OAM (0.2M), a mixture of OLA and OAM (1/1 vol/vol, ~0.4M), cesium oleate (0.2M + 0.25M OLA) and $CsPbBr_3$ NCs recorded in C_6D_6 (A) and $CDCl_3$ (B). The sample of cesium oleate was obtained from the same solution used for the NC synthesis.*

Figure 4A compares the ^{1}H-NMR spectrum of as-prepared $CsPbBr_3$ NCs in C_6D_6 with those of purified sample as well as of the relevant supernatant solution obtained after the isolation procedure by centrifugation. It can be noted that, apart from the reaction solvent (ODE), the first centrifugation removes the ligands and traces of the amide byproduct deriving from condensation between OLA and OAM. This species is characterized by the typical resonances at δ = 4.42 and 3.11 ppm, ascribable to –N*H*CO– and –C*H*$_2$NHCO– protons, respectively (supported by the HMBC spectrum in Figure S6). The purification by a single precipitation from hexane with an equivalent volume of acetone in the presence of ligands led to the complete removal of the amide, as testified by the absence of signals attributable to such species in the spectrum of the purified product. However, the supernatant solution obtained after the centrifugation prevalently contains the amide itself, hinting that the perovskite surface catalyzes the amide formation in the presence of a polar solvent, but that this impurity can be completely removed. Hence, it can be concluded that due to this surface-catalyzed amide formation, passivating ligands are easily lost during the purification procedures, even when a small amount of both OLA and OAM is added to preserve the NC integrity. Unfortunately, in the relevant ^{1}H NMR spectrum, the presence of the characteristic resonances of ODE at 4.94 and 5.8 ppm suggests an unsatisfactory purification of the sample from the reaction solvent. By carrying out only a further purification cycle, pure $CsPbBr_3$ NCs could be obtained, since ^{1}H-NMR reveals that ODE contamination can be totally removed from the sample. However, the relevant NC stability and solubility result to be severely compromised by the progressive elimination of ligands. The NMR characterization of this twice-purified $CsPbBr_3$ NCs sample is reported in Figure S7 along with the spectrum of the supernatant solution obtained from the isolation centrifugation.

The ^{1}H NMR spectrum of as-prepared $CsPbBr_3$ in C_6D_6 shows relatively broad signals, including the distinct resonance of the vinylene protons of the aliphatic chains (δ = 5.40÷5.70 ppm), but, with respect to other discriminating signals, these gain intensity due to their sufficient distance from the

NC surface. Hence, the chemical shift and broadening of the vinylene resonances are indicated to explore the bonding nature of the species passivating the NC surface. In fact, three contributions for the vinylene resonances can clearly be identified from inspection of Figure 4B, if one counts also the weak, slightly low-field shifted signal marked with an arrow at δ = 5.70 ppm. This observation implicates that solution NMR analysis can distinguish between three species interacting with the NC surface to a greater or lesser extent. By removing part of the organic shell, the first purification step does not alter the chemical composition of $CsPbBr_3$ NCs (as also confirmed by elemental analyses, *vide supra*) and the slight chemical shift variation of the main resonances (see Figure 4B) can be interpreted by the perturbation of the acid-base equilibrium due to the lower amount of the ligands engaged in passivation processes at the purified NC surface.

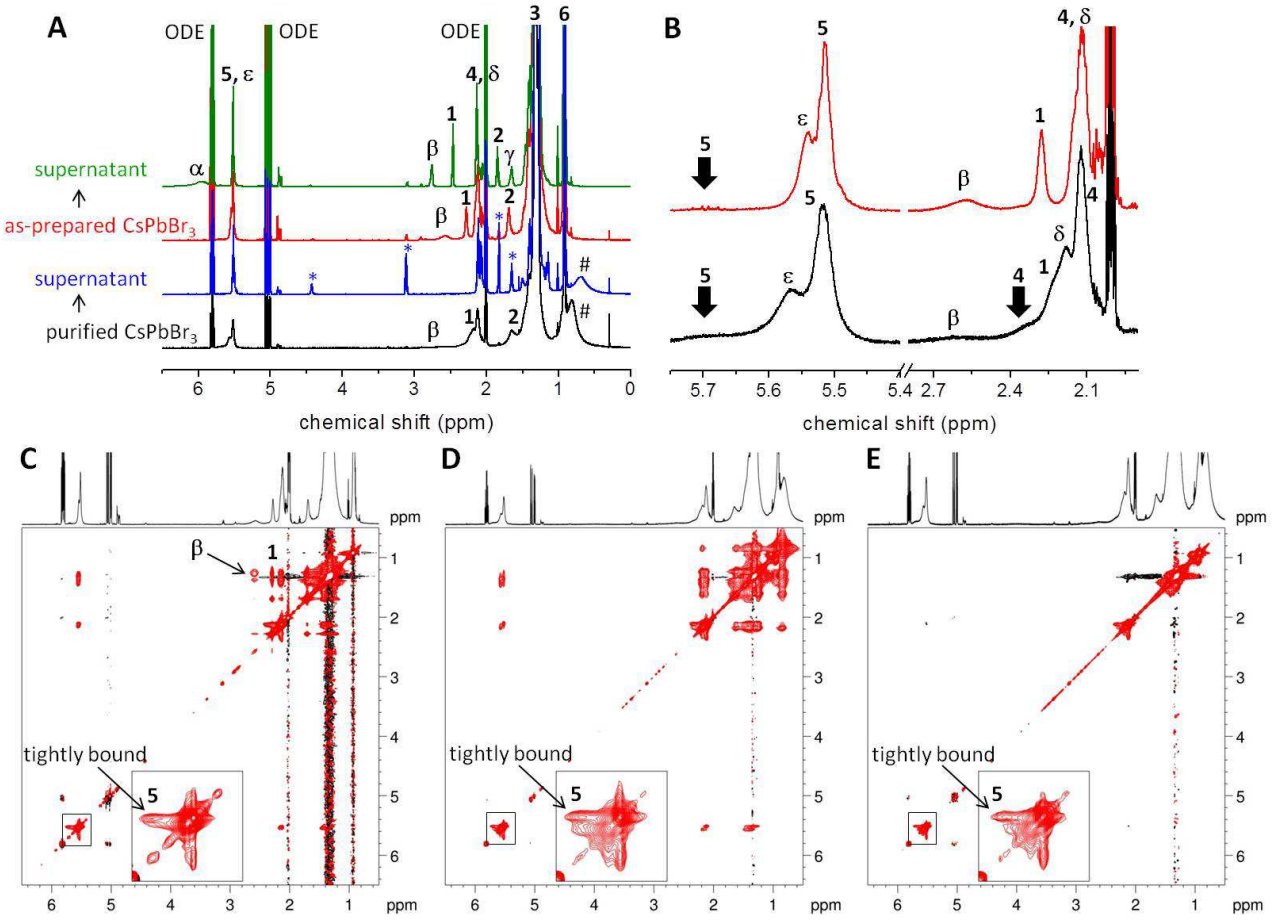

Figure 4. *(A) ^{1}H-NMR spectra of as-prepared and purified $CsPbBr_3$ NCs compared with the relevant supernatant solutions deriving from the product isolation by centrifugation. The resonances denoted with * correspond to the amide of OLA and OAM, while that marked with # is due to water. (B) Expansions of the same ^{1}H-NMR spectra of as-prepared and purified $CsPbBr_3$ NCs evidencing their main resonances. 2D NOESY spectrum of as-prepared (C) and purified (D) sample; the inset shows an expansion of the vinylene region. (E) ROESY spectrum of purified $CsPbBr_3$ NCs. All spectra are recorded in C_6D_6.*

The NOESY spectrum of the as-prepared sample in C_6D_6 (Figure 4C) confirms that ODE impurities are not bound to the $CsPbBr_3$ NCs showing positive (black) cross peaks, owing to lack of interaction with the surface. Concerning the ligands, cross-peaks connect different proton species involving cross-relaxation at some point of the molecules. Differently from what observed in previous investigations,[18] the NOESY spectrum of freshly as-prepared $CsPbBr_3$ NC indicates that OLA binds the surface in apolar solvent, as hinted by the appearance of negative (red in Figure 4C) cross-peaks attributable to the **1** resonance. Moreover, also the negative cross peaks observable between the OAM resonances corroborate its interaction with the surface. Since the downfield **1** resonances ascribable to OLA ligands are consequent to deprotonation reasonably due to the presence of a free base, we can infer that in apolar solvents one of the surface passivation involves adsorption/desorption processes of OAM rather than oleylammonium bromide. As schematized in Figure 2, the dissociation of the strong acid HBr from oleylammonium bromide in apolar solvents occurs with the support of the NC surface, freeing the corresponding amine, which can be engaged both in the passivation processes at the organic/inorganic interface as well as in the acid-base equilibria at the NC surroundings.

The nOe behaviour of the alkene resonances in as-prepared $CsPbBr_3$ NC (inset in Figure 4C) reveals negative cross peaks for the weak and broad resonance at δ = 5.70 ppm, confirming its

bound nature. We can anticipate that this broad resonance belongs to OLA bound fraction. Also, the sharper alkene resonances features negative nOe cross peaks and there is a cross peak from the broad to the sharp alkene resonance. We can conclude that the broad resonance is due to tightly bound ligands, in slow exchange with weakly bound ligands, featuring sharp resonances.[40,41] In the case of as-prepared $CsPbBr_3$, the cross-peak between the vinylene protons **5** derives from the connection between bound and free OLA species (inset of Figure 4C). The same interactions are also present in the case of the purified sample (Figure 4D), where a cross-peak between tightly bound **5** and **ε** resonance of OAM can additionally be noted. These interactions can either originate from intramolecular cross-relaxation between the vinylene protons of neighboring molecules or result from the simple exchange of molecules between the pool of bound and free OLA. While NOESY cannot distinguish cross-relaxation from chemical exchange, rotating-frame nuclear Overhauser effect spectroscopy (ROESY) spectrum of purified $CsPbBr_3$ NCs (Figure 4E) evidences negative cross-peaks between signals attributable to tightly and weakly bound OLA molecules. This means that this cross-peak mainly originates from the slow exchange between the pools of tightly bound and excess OLA (at δ = 5.52 ppm), while the third species (δ = 5.57 ppm) attributable to the observed vinylene resonances corresponds to the amine compounds in fast exchange between bound and free states. The presence of tightly bound OLA was also observed by Brutchey *et al.* in $CsPbBr_3$ NCs purified without the support of ligands.[42]

The ^{1}H-NMR spectra recorded in the polar solvent ($CDCl_3$) of both as-prepared and purified $CsPbBr_3$ NCs are reported in Figure 5A, revealing the presence of a relatively broad resonance attributable to weakly bound OLA. The interaction of OLA with the surface is confirmed by the relevant NOESY spectra, which showcase negative cross-peaks for **1** and **2** protons both in as-prepared and purified sample (Figure 5B and C). On the other hand, the entity of the downfield-shift of the **β** protons resonance reasonably suggests that OAM is more protonated and exhibited a negative cross-peak (more evident in the case of purified sample) in the relevant NOESY spectra,

suggesting that this species is interacting with the NC surface. Differently from what recorded in the apolar C_6D_6, no signals attributable to tightly bound OLA species could be observed. We can infer that also in the polar solvent the stabilization mechanism promoted by the aliphatic amine is highly dynamic, but the exchange process at the NC surface involving OLA is faster with respect to that observed in apolar solvents. The dynamic stabilization in polar solvents promotes desorption of oleylammonium bromide with consequences on the surface chemistry and stability of the relevant purified NCs.

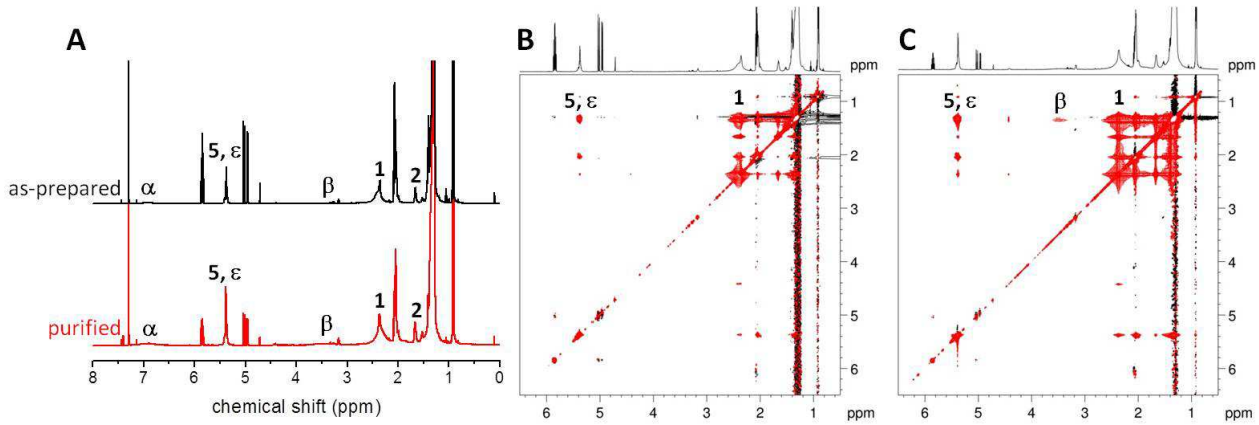

Figure 5. *(A) Comparison between the ^{1}H-NMR spectra of as-prepared and purified $CsPbBr_3$ NCs in $CDCl_3$; 2D NOESY spectrum of as-prepared (B) and purified (C) sample.*

To support our findings, we measured DOSY spectra of purified $CsPbBr_3$ NCs in the two aforementioned solvents (C_6D_6 and $CDCl_3$). By focusing on the vinylene resonances and using a biexponential fitting, we obtained two different diffusion coefficients ($D = 5.7 \times 10^{-10}$ m^2/s and 8.1×10^{-10} m^2/s for OAM and OLA, respectively) in C_6D_6 effectively attributable to the ligands engaged in the passivation process. In fact, these values are smaller than those of the relevant free species ($D \approx 1.0 \times 10^{-9}$ m^2/s), but remarkably higher than those evaluated from TEM measurements ($D = 5.1 \times 10^{-11}$ m^2/s),[18] ascribable to tightly bound ligands, because of the very low-intensity of their NMR signal hampering the extrapolation of their diffusion coefficient. This observation

implies that OAM is not tightly bound to the NC surface but is subject to a fast exchange between its bound and free state; as a consequence, an average diffusion coefficient between the two situations appears in the DOSY spectrum. Conversely, OLA slowly exchanges with bound ligands (suggested by the aforementioned broad resonances at δ = 5.65 ppm) and its diffusion coefficient is near to that of free molecules. In the polar medium, we observed an analogous situation, since two species are evident with diffusion coefficients ($D = 3.3 \times 10^{-10}$ m^2/s and 8.8×10^{-10} m^2/s for OAM and OLA, respectively) incompatible with the average NC dimensions. Furthermore, the found values are smaller than the diffusion coefficients of the relevant free species ($D \approx 9.0 \times 10^{-10}$ m^2/s) and the slower diffusion for the amine species suggests that the interaction of oleylammonium bromide with the NC surface in $CDCl_3$ is stronger than that of OAM in the apolar solvent.

Degradation pathway of the organic shell in $CsPbBr_3$ NCs. Concerning the crucial issue of perovskite NC stability, we analyzed the ^{1}H-NMR spectrum of as-prepared $CsPbBr_3$ NCs stored in C_6D_6 solution at ambient conditions for three weeks (Figure 6A). Inspection of the solution after three weeks revealed the incipient formation of a yellow precipitate, strongly hinting transformations of the nanomaterial, which compromise its colloidal stability. It is reasonable to suppose that these transformations involve the NC surface favouring aggregation between nanoparticles. Actually, the appearance of new signals attributable to the amide formation from the condensation of OLA and OAM is evident, while the disappearance of the amine resonances is probably related to the complete conversion into the amide (Figure 6A). Since the relevant NOESY spectrum exhibits positive (black) cross-peaks in Figure 6B for the amide, one can conclude that this species is not interacting with the NC surface and that this degradation pathway depauperates the surface of passivating agents lowering the NC colloidal stability. The same reactivity was observed in the case of the purification step (*vide supra*) when acetone was added to the NC solution. While engaging the passivation process, oleylammonium species can release protons to the

NC surface, as suggested by the ^{1}H-NMR analysis of the $CsPbBr_3$ nanomaterial (*vide supra*). We suspect that the acid surface of the perovskite NCs is responsible for the amide evolution as schematized in Figure 6C, because the mixture of OLA and OAM (in the absence of $CsPbBr_3$ NCs) stored in the same conditions did not evidence the amide formation.[43] The catalytic effect of the nanomaterial is due to the affinity of both ligands toward its surface, promoting the spatial proximity necessary for the condensation. Concerning the degradation mechanism, it is reasonable to suppose that the interaction of the surface protons with the carboxylic groups approaching to the nanomaterial increases their electrophilicity, thus favouring the amine attack and promoting the amide formation. At the same time, the amide evolution is noticeably slowed down in the case of purified $CsPbBr_3$ NCs stored at ambient conditions for three weeks (Figure S8), thus explaining their higher stability. On these bases, we can rationalize the impact of purification on the colloidal stability of the resulting NCs. As-prepared samples suffer from degradation of the organic shell compromising NC colloidal stability, probably due to adsorbed protons or other unwashed Lewis acidic species (metal precursors or intermediates) which catalyze ligand condensation. The first purification step, carried out with acetone removes most of adsorbed-acidic species from the NC surface, thus inhibiting this degradation pathway in the purified material. Although the above-mentioned degradation pathway is extremely slow at room temperature, anyhow it is sufficient to induce the colloidal instability of the corresponding nanomaterial.

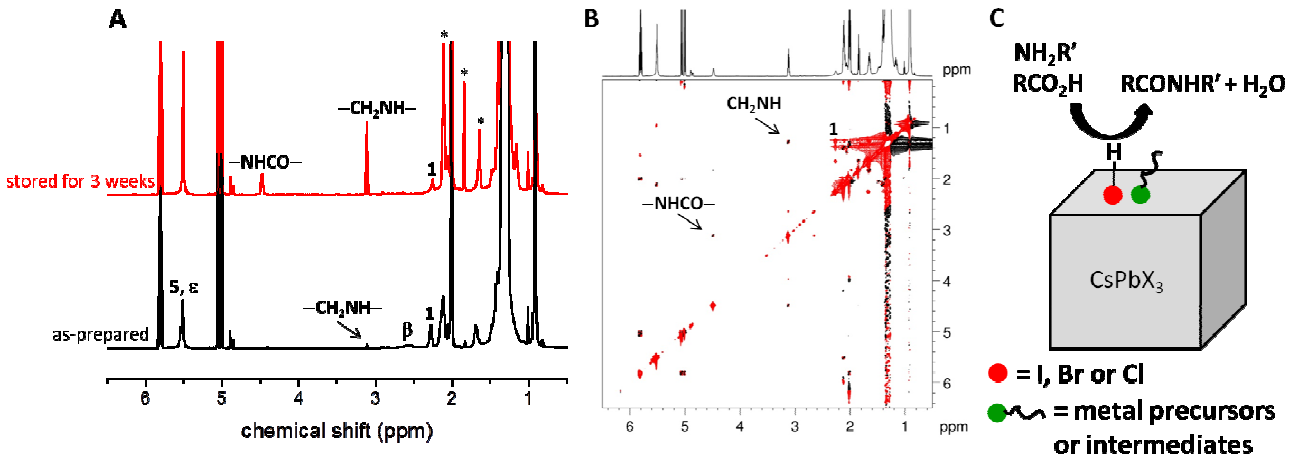

Figure 6. *(A) Comparison between the ^{1}H-NMR spectra in C_6D_6 of as-prepared $CsPbBr_3$ NCs and the same sample stored for three weeks under ambient conditions and room lighting. Along with the characteristic signals of –NHCO– and –CH_2NHCO– protons, the resonances denoted with * are fingerprints of the amide evolution. (B) 2D-NOESY spectrum of degraded sample. (C) Schematic representation of amide evolution catalyzed by absorbed acidic species on the perovskite NC surface.*

Surface chemistry of $CsPbX_3$ NCs. The surface chemistry of as-synthesized $CsPbCl_3$ and $CsPbI_3$ was compared to that of $CsPbBr_3$ and the relevant ^{1}H-NMR spectra in C_6D_6 are shown in Figure 7A. Apparently, the ^{1}H-NMR spectrum of $CsPbCl_3$ is very similar to that of $CsPbBr_3$. Considering that all $CsPbX_3$ NCs of this study have been submitted to the same reaction condition and the same isolation procedures, the main aspect emerging from the comparison between the spectra of the three NCs is the presence of a large amount of amide contaminating the $CsPbI_3$ sample, which, by contrast, is negligible in the other two samples. We ascertained that the amide evolution is not occurring at the early stage of the reaction by sampling an aliquot of PbI_2/OLA/OAM mixture immediately before the addition of cesium-oleate solution (Figure S9). On the basis of the previously described correlation between amide formation and NC stability, the rapid amide evolution in $CsPbI_3$ NCs is a hint of an incipient degradation of the organic shell protecting these nanomaterials. Since the solution NMR spectrum was recorded immediately after the NC isolation it can be stated that a fast degradation occurs for this material. The rationale for this peculiar behavior observed for $CsPbI_3$ NCs might be found in the “soft” character of the iodine atoms that could favour the interaction of OLA molecules with the surface through secondary bond interactions with the COOH groups.[44] If OLA interacts more strongly with the NC surface, the catalytic condensation with OAM yielding the corresponding amide would be reasonably favored.

Noticeably, the weak resonances ascribable to OLA and OAM in $CsPbI_3$ (Figure 7B) are remarkably downfield shifted with respect to the corresponding resonances of $CsPbCl_3$ and $CsPbBr_3$ NCs in the apolar solvent. The position of the broad signal attributable to **β** resonance (δ = ~2.85 ppm) suggests a large protonation of OAM passivating the NC surface, while the chemical shift of **1** resonance (δ = 2.38 ppm) hints that OLA is largely deprotonated, if compared with the signals in $CsPbCl_3$ and $CsPbBr_3$ NCs. Indeed, the **1** resonance perfectly coincides with that of cesium-oleate both in C_6D_6 and $CDCl_3$ (Figure S10). Since the compositional analysis of $CsPbI_3$ NCs points to a Cs-rich surface, we can conclude that the surface passivation of $CsPbI_3$ NCs is due to the competition between oleylammonium iodide and cesium-oleate both in apolar and in polar solvents, which effectively results extremely labile (see also the schematic picture of Figure 8C). Since most of the ligands are consumed in the formation of the inert amide, the NC surface is heavily exposed to structural decomposition induced by interaction with polar solvents or ambient moisture.

The NOESY spectrum of the as-prepared $CsPbCl_3$ NC reveals tightly bound species with negative cross peaks in analogy with the $CsPbBr_3$ counterpart. The sharper vinylene resonance also features negative nOe cross peaks and the spectrum displays also a cross peak from the broad to the sharp **5** resonance, most probably due to chemical exchange (see inset Figure 7C). By contrast, the tightly bound species are not detected in the case of $CsPbI_3$ NCs, while negative cross-peaks are evident for the resonances attributable to cesium-oleate indicating some interaction with the surface. Moreover, the amide byproduct gave positive cross-peaks confirming the absence of interaction with the surface as in the case of ODE. These results support the hypothesis that both in apolar and polar solvents cesium-oleate and oleylammonium iodide are the species engaged in surface passivation. Conversely, the stronger Pb–Cl and Pb–Br bonds hamper the dissociation of the corresponding ammonium salts in apolar solvents and, at the same time, offer the appropriate

substrate for the interaction with cesium cations, which, in turn, can firmly bind oleate moieties to the NC surface.

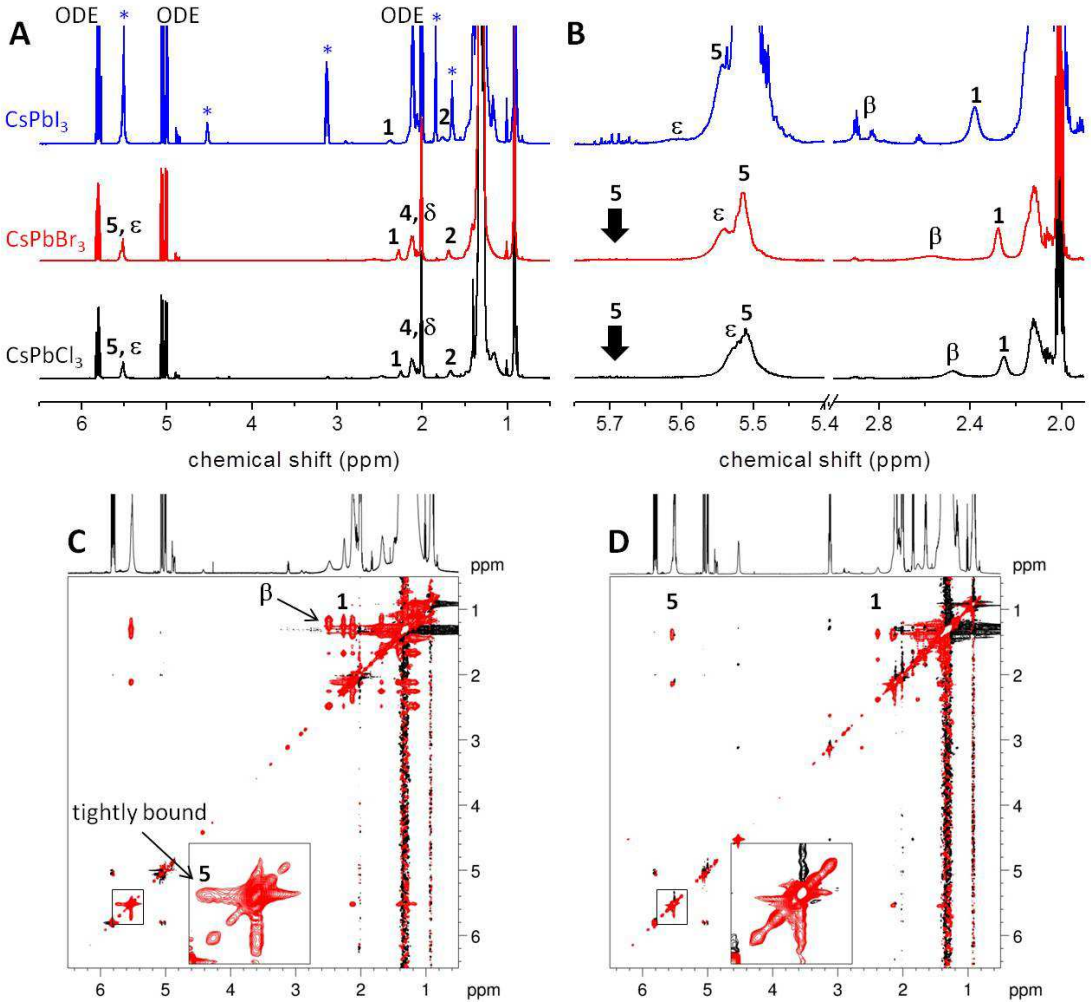

Figure 7. *(A) ^{1}H-NMR spectra in C_6D_6 of as-prepared $CsPbBr_3$ NCs compared with $CsPbCl_3$ and $CsPbI_3$ NCs. The resonances denoted with * correspond to the amide of OLA and OAM. (B) Expansions of the same ^{1}H-NMR spectra in the region of the main observable resonances. 2D NOESY spectrum of as-prepared $CsPbCl_3$ (C) and $CsPbI_3$ (D) NCs.*

Since as-prepared $CsPb(I/Br)_3$ NCs exhibited a halide composition (*vide supra*) far from the equimolar ratio of the precursor feed used for the synthesis (as obtained for example in

$CsPb(Br/Cl)_3$ NCs, Figure S11), we deemed it worthwhile to explore the surface chemistry of mixed-halide perovskite nanomaterials on the basis of the knowledge gained on the relevant single-halide materials. Starting from the element composition of $CsPb(I/Br)_3$ NCs, the lower amount of iodine can tentatively be explained by the competition between iodine and bromine ions for the incorporation in the crystal lattice, disfavoring the larger iodide ions. If this hypothesis is true, we would expect an excess iodine on the relevant mixed-halide NC surface. As a matter of fact, we observed that ^{1}H-NMR spectrum of as-prepared $CsPb(I/Br)_3$ NCs is very similar to that of $CsPbI_3$ NCs, suggesting that the mixed-halide material exposes a I-rich surface (Figure 8A). In fact, all the peculiarities of a I-rich surface are observed: a large quantity of formed amide, weak signals attributable to ligands, the simultaneous presence of oleylammonium and cesium-oleate, the absence of tightly bound oleate (Figure S12). The poorer binding efficiency of the surface passivating agents in nanoparticles with an iodide-rich character was also observed in mixed-halide $CsPbBr_{3-x}I_x$ nanocrystals obtained upon modification of the surface composition of pristine $CsPbBr_3$ nanoparticles by adding a suitable iodide source.[45]

The purification changes on the compositional and optical properties of purified $CsPb(I/Br)_3$ NCs are reflected on their surface chemistry. Recalling that all syntheses and purifications were carried out by using the same amounts of reactants and solvents, the ^{1}H-NMR spectrum of purified $CsPb(I/Br)_3$ NCs shows relatively intense signals attributable to the ligands, although the amide impurity was not completely removed by the purification. The inspection on the vinylene cross-peaks in 2D-NOESY spectrum of this sample evidences the presence of tightly bound oleate and weakly interacting passivating agents (Figure 8B). If dangling iodides are removed in the course of purification, the new surface now exposes strongly bound cesium and undercoordinated lead atoms, which are promptly passivated by OAM and OLA (Figure 8C). The more efficient passivation is explicated by the higher colloidal stability of the resulting purified sample. Indeed, a solution of

purified $CsPb(I/Br)_3$ NCs stored for 3 weeks in ambient conditions appears as clear, while a suspension is formed in the case of an unpurified sample (see Figure 8D).

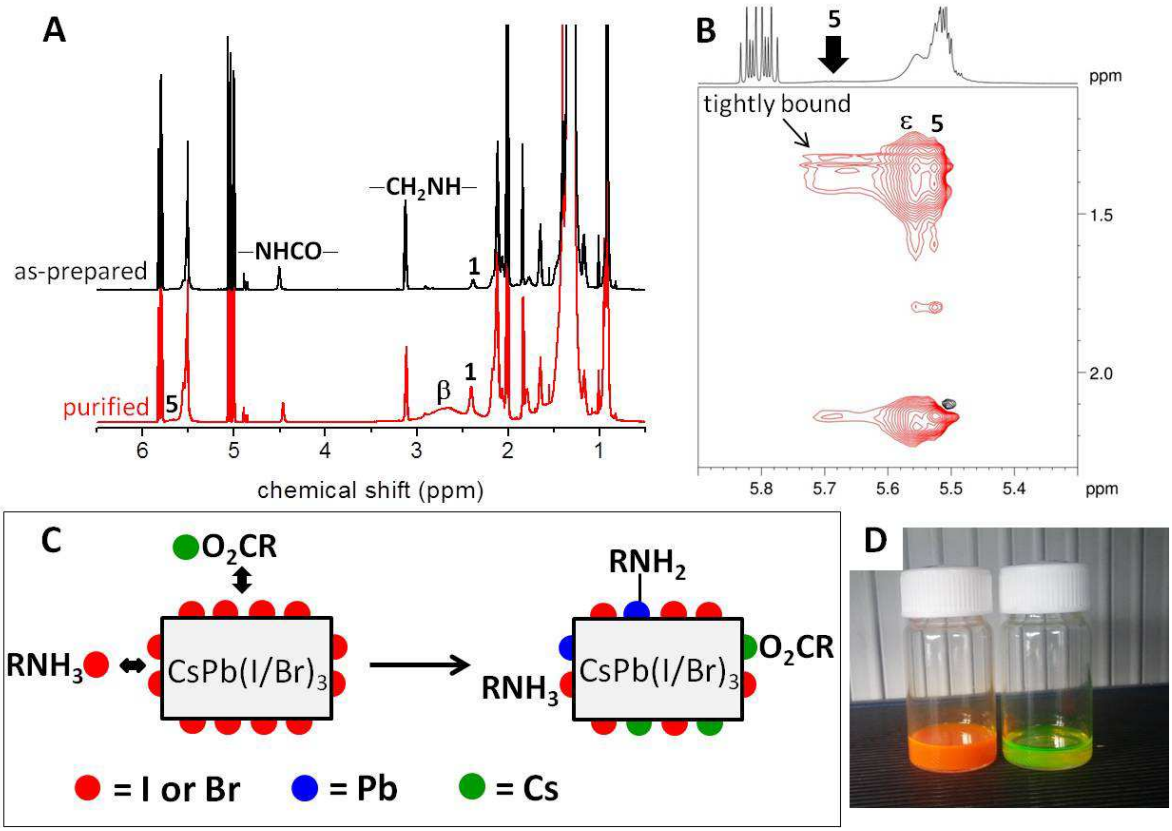

Figure 8. *(A) ^{1}H-NMR spectrum in C_6D_6 of as-prepared $CsPb(I/Br)_3$ NCs compared with that of the relevant purified sample . (B) 2D NOESY spectrum of purified $CsPb(I/Br)_3$ NCs. (C) Schematic picture illustrating the NC surface modification upon purification. (D) Solutions of as-prepared (left) and purified (right) $CsPb(I/Br)_3$ NCs dissolved in cyclohexane and stored in ambient conditions for three weeks under room lighting conditions.*

CONCLUSIONS

This study aimed at unraveling the surface chemistry of $CsPbX_3$ NCs pointing to disentangle the open issues regarding their instability and the necessity of a purification step after their preparation. The colloidal NCs under investigation were prepared by traditional hot-injection methods with a

different halide composition and were systematically analyzed for their elemental composition, morphology, crystalline structure and optical properties. Concerning the need for a purification step, we ascertained that addition of small amounts of OLA and OAM before precipitation with acetone preserves the colloidal integrity of the NCs, except for the case of $CsPbI_3$ NCs, which undergo a fast phase transition immediately after the contact with the polar solvent. We were pleased to ascertain a higher phase purity of the all other purified perovskite samples, which comes along with quantum yields substantially unaltered with respect to as-prepared samples. A further purification step did afford practically uncontaminated samples, but resulted to be deleterious for the long-term colloidal stability of the NCs. A thorough NMR investigation allowed us to establish the $CsPbX_3$ surface as governed by the following species and equilibria in apolar solvents:

1) strongly bound oleate species likely anchored to undercoordinated lead or cesium atoms;

2) formal oleylamine weakly bound through protons of the NC surface and undercoordinated lead atoms.

3) carboxylic acid exchanging with tightly bound oleate, a process favored by desorbed amine.

When the perovskite NCs were dissolved in polar solvents, we observed a modification of the equilibria at the basis of NC surface passivation in favor of the oleylammonium halide desorption from the surface. We gained insight into the origin of the long-term colloidal instability of $CsPbX_3$ NCs by ascertaining the evolution of the amide formed by condensation of carboxylic acid and aliphatic amine in the case of the as-prepared samples, which is catalyzed by the acid NC surface. The single purification step with a polar antisolvent removed adsorbed protons from the NC surface as the corresponding oleylammonium halide leading to a long-term stable nanomaterial. In the case of I-containing NCs, we observed their surface passivated by oleylammonium halide and cesium-oleate both in apolar and in polar solvents. The I-rich surface of these NCs favored the acid-catalyzed amide evolution which depauperates the nanomaterial of the organic passivating shell,

thus explaining their pronounced instability in the presence with polar solvents. Although the structural stability of perovskite NCs is very likely a multifaceted problem involving not only the surface equilibria of the organic ligands but also other factors, such as halide equilibrium,[46] in perspective, the insights reported in this study support the critical need for a NC passivation strategy with surface ligands that are also compatible with the charge transport requirements of optoelectronic applications.

EXPERIMENTAL SECTION

Materials. Cesium carbonate (Cs_2CO_3, 99.9% metals basis, Alfa Aesar), lead(II) bromide ($PbBr_2$, 99.999% metals basis, Aldrich), lead(II) chloride ($PbCl_2$, 99.999% metals basis, Aldrich), lead(II) iodide (PbI_2, 99.999% metals basis, Aldrich), oleylamine (OAM, technical grade 70%, Aldrich), oleic acid (OLA, technical grade 90%, Aldrich), 1-octadecene (ODE, technical grade 90%, Aldrich), acetone (ACS grade), hexane (VWR, LC-MS grade), cyclohexane (Aldrich, spectrophotometric grade).

Synthesis of as-prepared $CsPbX_3$ NCs. All manipulations were performed under nitrogen flow using standard Schlenk techniques. Cs_2CO_3 (0.407 g, 1.25 mmol), OLA (1.55 mL, 4.91 mmol) and ODE (20 mL) were mixed in a 50 mL Schlenk tube and kept in vacuum for 1 hour at 120 °C. Later the tube was filled with nitrogen for complete solubilization of the solid material, which leads to the formation of a clear solution of cesium oleate (Cs-oleate). As Cs-oleate precipitates out of ODE at room temperature, it was kept at 120 °C under N_2 atmosphere before injection. ODE (7.5 mL), PbX_2 (0.38 mmol), OLA (1.0 mL) and OAM (1.0 mL) were loaded in a 50 mL Schlenk tube and the mixture was heated at 160°C. After complete solubilization of the PbX_2 salt, temperature was kept for 20 minutes followed by injection of Cs-oleate solution (0.8 mL). The reaction mixture was cooled in an ice-water bath after 5 s. The crude solution was centrifuged at 4000 rpm for 40 min.

The supernatant containing unreacted precursors was discarded and obtained precipitate was finally dispersed in cyclohexane for measurements.

Purified $CsPbX_3$ NCs. In the case of purification, the precipitate obtained after the first centrifugation was dissolved in hexane (1.2 mL). Next, 50 μl of OLA and OAM were added to the suspension before the addition of acetone (not dried, 1.2 mL). After centrifugation (4000 rpm for 10 min), the supernatant was discarded, and the precipitate was redispersed in cyclohexane for subsequent characterization.

Nuclear Magnetic Resonance. ^{1}H-NMR spectra of samples dissolved in N_2-saturated solution were recorded at 298.2 K on a Bruker Avance III 700 MHz spectrometer equipped with a Cryoprobe optimized for ^{1}H observation. All NMR chemicals shifts were referred to the non-deuterated benzene or chloroform residue peak at 7.16 ppm and 7.26 ppm, respectively. The NOESY and ROESY spectra were acquired using standard pulse sequences; NOESY and ROESY mixing times were set to 300 ms and 200 ms, respectively. The DOSY measurements were performed using standard pulse sequences. In order to keep a constant time of measurement throughout all the experiments, the diffusion time (Δ) and the diffusion gradient length (δ) were set to 100 ms and 5 ms, respectively and kept constant. The gradient strength was linearly increased in 16 steps and monitored by the attenuation (from 2% to 95%) of the first increment signal. The diffusion coefficients were obtained by fitting the appropriate Stejskal−Tanner equation to the signal intensity decay.[47]

Optical characterization. UV–vis absorption spectra were collected using a Jasco V670 spectrometer in transmission mode. Steady-state PL spectra from solutions were acquired on Varian Cary Eclipse instrument. The quantum yields were determined using appropriate dye references for blue, green and red spectral regions (coumarin 343, fluorescein, and rhodamine 6G, respectively) according to standard procedures.[48]

TEM characterization. Transmission electron microscopy (TEM) measurements were carried out using a JEOL JEM1011 microscope, operating at an accelerating voltage of 100 kV and equipped with a tungsten electron source, and CCD high resolution camera. Samples for TEM analysis were prepared by dipping the carbon-coated copper grid into the NC cyclohexane solution diluted with anhydrous hexane. Statistical analysis of the size (NC average size and standard deviation) of each sample was performed by using a freeware image analysis program, by measuring more than 200 of nanoparticles.

FEG-SEM-EDX. Elemental analyses were performed using a field emission gun scanning electron microscope (FEG-SEM) Zeiss Σigma 300 VP (Zeiss Oberkochen, Germany) equipped with an energy dispersive spectrometer (EDX) C-MaxN SDD with an active area of 20 mm^2 (Oxford Instruments, Oxford, United Kingdom). NC solutions in cyclohexane were deposited on aluminum stubs covered with a pure graphite tape. Analysis were carried out at 15kV using a 7.5 mm working distance at a magnification of 1000×. The data accuracy was checked using standards by MAC (Micro-Analysis Consultants Ltd., United Kingdom).

X-Ray Diffraction. XRD data were collected in detector scan mode or coupled sample-detector scan mode, by a Bruker D8 Discover equipped with a Cu source (Kα line), a Göbel mirror, and a scintillation point detector.

ACKNOWLEDGMENTS

M.I.-V., R.G. and G.P.S. acknowledge the Bridge-Early Stage COMPOSTRONICS project (cod. 5730587, Austrian Research Promotion Agency-FFG) for funding. R.G. and G.P.S. acknowledge Apulia Region for project “Nanoapulia– nanofotocatalizzatori per un’atmosfera più pulita” (Bando Aiuti a Sostegno dei Cluster Tecnologici Regionali - cod. MDI6SR1) and Italian MIUR for project MAAT (Molecular NAnotechnology for HeAlth and EnvironmenT - PON02_00563_3316357).

Rocco Lassandro is acknowledged for technical support during XRD data collection. FEG-SEM-EDX measurements were performed at Micro X-ray Lab (www.microxraylab.com).

Conflicts of interest. There are no conflicts to declare.

Electronic Supplementary Information. Additional characterization and images of NCs.

REFERENCES

[1] N. J. Jeon, J. H. Noh, W. S. Yang, Y. C. Kim, S. Ryu, J. Seo and S. I. Seok, *Nature*, 2015, **517**, 476–481.

[2] Z.-K. Tan, R. S. Moghaddam, M. L. Lai, P. Docampo, R. Higler, F. Deschler, M. Price, A. Sadhanala, L. M. Pazos, D. Credgington, F. Hanusch, T. Bein, H. J. Snaith and R. H. Friend, *Nat. Nanotechnol.*, 2014, **9**, 687−691.

[3] Q. A. Akkerman, G. Rainò,M. V. Kovalenko and L. Manna, *Nat. Mater.*, 2018, **17**, 394–405.

[4] Q. Zhang and Y. Yin, *ACS Cent. Sci.*, 2018, **4**, 668–679.

[5] J. Butkus, P. Vashishtha, K. Chen, J. K. Gallaher, S. K. K. Prasad, D. Z. Metin, G. Laufersky, N. Gaston, J. E. Halpert and J. M. Hodgkiss, *Chem. Mater.*, 2017, **29**, 3644−3652.

[6] J. Z. Song, J. H. Li, X. M. Li, L. M. Xu, Y. H. Dong and H. B. Zeng, *Adv. Mater.*, 2015, **27**, 7162−7167.

[7] Q. A. Akkerman, V. D'Innocenzo, S. Accornero, A. Scarpellini, A. Petrozza, M. Prato and L. Manna, *J. Am. Chem. Soc.*, 2015, **137**, 10276–10281.

[8] L. Protesescu, S. Yakunin, M. I. Bodnarchuk, F. Krieg, R. Caputo, C. H. Hendon, R. X. Yang, A. Walsh and M. V. Kovalenko, *Nano Lett.*, 2015, **15**, 3692–3696.

[9] Y. Kim, E. Yassitepe, O. Voznyy, R. Comin, G. Walters, X. W. Gong, P. Kanjanaboos, A. F. Nogueira and E. H. Sargent, *ACS Appl. Mater. Interfaces*, 2015, **7**, 25007–25013.

[10] M. A. Boles, D. Ling, T. Hyeon and D. V. Talapin, *Nat. Mater.*, 2016, **15**, 141–153.

[11] D. Yang, X. Li and H. Zeng, *Adv. Mater. Interfaces*, 2018, **5**, 1701662.

[12] A. Swarnkar, A. R. Marshall, E. M. Sanehira, B. D. Chernomordik, D. T.; Moore, J. A. Christians, T. Chakrabarti and J. M. Luther, *Science*, 2016, **354**, 92–95.

[13] D. M. Trots and S. V. Myagkota, *J. Phys. Chem. Solids*, 2008, **69**, 2520–2526.

[14] L. Protesescu, S. Yakunin, S. Kumar, J. Bär, F. Bertolotti, N. Masciocchi, A. Guagliardi, M. Grotevent, I. Shorubalko, M. I. Bodnarchuk, C.-J. Shih and M. V. Kovalenko, *ACS Nano*, 2017, **11**, 3119–3134.

[15] C. Wang, A. S. R. Chesman and J. J. Jasieniak, *Chem. Commun.*, 2017, **53**, 232–235.

[16] F. Liu, Y. Zhang, C. Ding, S. Kobayashi, T. Izuishi, N. Nakazawa, T. Toyoda, T. Ohta, S. Hayase, T. Minemoto, K. Yoshino, S. Dai and Q. Shen, *ACS Nano*, 2017, **11**, 10373–10383.

[17] M. Imran, V. Caligiuri, M. Wang, L. Goldoni, M. Prato, R. Krahne, L. De Trizio and L. Manna, *J. Am. Chem. Soc.*, 2018, **140**, 2656–2664.

[18] J. De Roo, M. Ibáñez, P. Geiregat, G. Nedelcu, W. Walravens, J. Maes, J. C. Martins, I. Van Driessche, M. V. Kovalenko and Z. Hens, *ACS Nano*, 2016, **10**, 2071–2081.

[19] A. Pan, B. He, X. Fan, Z. Liu, J. J. Urban, A. P. Alivisatos, L. He and Y. Liu, *ACS Nano*, 2016, **10**, 7943–7954.

[20] T. Udayabhaskararao, L. Houben, H. Cohen, M. Menahem, I. Pinkas, L. Avram, T. Wolf, A. Teitelboim, M. Leskes, O. Yaffe, D. Oron and M. Kazes, *Chem. Mater.*, 2018, **30**, 84–93.

[21] Z. Liu, Y. Bekenstein, X. Ye, S. C. Nguyen, J. Swabeck, D. Zhang, S.-T. Lee, P. Yang, W. Ma and A. P. Alivisatos, *J. Am. Chem. Soc.*, 2017, **139**, 5309–5312.

[22] J. Pan, Y. Shang, J. Yin, M. De Bastiani, W. Peng, I. Dursun, L. Sinatra, A. M. El-Zohry, M. N. Hedhili, A.-H. Emwas, O. F. Mohammed, Z. Ning and O. M. Bakr, *J. Am. Chem. Soc.*, 2018, **140**, 562–565.

[23] Z. Hens and J. C. Martins, *Chem. Mater.*, 2013, **25**, 1211–1221.

[24] I. Moreels, B. Fritzinger, J. C. Martins and Z. Hens, *J. Am. Chem. Soc.*, 2008, **130**, 15081–15086.

[25] B. Fritzinger, I. Moreels, P. Lommens, R. Koole, Z. Hens and J. C. Martins, *J. Am. Chem. Soc.*, 2009, **131**, 3024–3032.

[26] H. Liu, Z. Wu, H. Gao, J. Shao, H. Zou, D. Yao, Y. Liu, H. Zhang and B. Yang, *ACS Appl. Mater. Interfaces*, 2017, **9**, 42919–42927.

[27] A. Altomare, C. Cuocci, C. Giacovazzo, A. Moliterni, R. Rizzi, N. Corriero, A. Falcicchio, *J. Appl. Cryst.*, 2013, **46**, 1231–1235.

[28] B. A. Koscher, J. K. Swabeck, N. D. Bronstein and A. P. Alivisatos, *J. Am. Chem. Soc.*, 2017, **139**, 6566–6569.

[29] J. Pan, S. P. Sarmah, B. Murali, I. Dursun, W. Peng, M. R. Parida, J. Liu, L. Sinatra, N. Alyami, C. Zhao, E. Alarousu, T. K. Ng, B. S. Ooi, O. M. Bakr and O. F. Mohammed, *J. Phys. Chem. Lett.*, 2015, **6**, 5027–5033.

[30] V. K. Ravi, P. K. Santra, N. Joshi, J. Chugh, S. K. Singh, H. Rensmo, P. Ghosh and A. Nag, *J. Phys. Chem. Lett.*, 2017, **8**, 4988–4994.

[31] J. Maes, L. Balcaen, E. Drijvers, Q. Zhao, J. De Roo, A. Vantomme, F. Vanhaecke, P. Geiregat and Z. Hens, *J. Phys. Chem. Lett.*, 2018, **9**, 3093–3097.

[32] S. ten Brinck and I. Infante, *ACS Energy Lett.*, 2016, **1**, 1266–1272.

[33] Q. Jing, M. Zhang, X. Huang, X. Ren, P. Wang and Z. Lu, *Nanoscale*, 2017, **9**, 7391–7396.

[34] J. De Roo, I. Van Driessche, J. C. Martins and Z. Hens, *Nat. Mater.*, 2016, **15**, 517–522.

[35] J. Pan, L. N. Quan, Y. Zhao, W. Peng, B. Murali, S. P. Sarmah, M. Yuan, L. Sinatra, N. M. Alyami, J. Liu, E. Yassitepe, Z. Yang, O. Voznyy, R. Comin, M. N. Hedhili, O. F. Mohammed, Z. H. Lu, D. H. Kim, E. H. Sargent and O. M. Bakr, *Adv. Mater.*, 2016, **28**, 8718–8725.

[36] N. C. Anderson, M. P. Hendricks, J. J. Choi and J. S. Owen, *J. Am. Chem. Soc.*, 2013, **135**, 18536–18548.

[37] J. De Roo, N. Yazdani, E. Drijvers, A. Lauria, J. Maes, J. S. Owen, I. Van Driessche, M. Niederberger, V. Wood, J. C. Martins, I. Infante and Z. Hens, *Chem. Mater.* 2018, **30**, 5485–5492.

[38] R. Grisorio, D. Debellis, G. P. Suranna, G. Gigli and C. Giansante, *Angew. Chem. Int. Ed.*, 2016, **55**, 6628–6633.

[39] G. Almeida, L. Goldoni, Q. Akkerman, Z. Dang, A. H. Khan, S. Marras, I Moreels and L. Manna, *ACS Nano*, 2018, **12**, 1704–1711.

[40] B. Fritzinger, R. K. Capek, K. Lambert, J. C. Martins and Z. Hens, *J. Am. Chem. Soc.*, 2010, **132**, 10195–10201.

[41] C. N. Valdez, A. M. Schimpf, D. R. Gamelin and J. M. Mayer, *ACS Nano*, 2014, **8**, 9463–9470.

[42] S. R. Smock, T. J. Williams and R. L. Brutchey, *Angew.Chem. Int .Ed.* 2018, **57**,11711–11715.

[43] J. De Roo, E. A. Baquero, Y. Coppel, K. De Keukeleere, I. Van Driessche, C. Nayral, Z. Hens and F. Delpech, *ChemPlusChem*, 2016, **81**, 1216–1223.

[44] V. González-Pedro, S. A. Veldhuis, R. Begum, M. J. Bañuls, A. Bruno, N. Mathews, S. Mhaisalkar and A. Maquieira, *ACS Energy Lett.*, 2018, **3**, 1409–1414.

[45] E. G. Ripka, C. R. Deschene, J. M. Franck, I.-T. Bae and M. M. Maye, *Langmuir* 2018, **34**, 11139–11146.

[46] Y. Dong, T. Qiao, D. Kim, D. Parobek, D. Rossi, D. H. Son, *Nano Lett.*, 2018, **18**, 3716–3722.

[47] E. O. Stejskal and J. E. Tanner, *J. Chem. Phys.*, 1965, **42**, 288–292.

[48] M. Grabolle, M. Spieles, V. Lesnyak, N. Gaponik, A. Eychmüller and U. Resch-Genger, *Anal. Chem.*, 2009, **81**, 6285–6294.